Nighttime Light Data and Spatial Modeling for Land-Use Carbon Emissions: Insights from Northeast China

Jie Wang, Qiuyun Liu, Lulu Zhang，Mingyu Li*

College of Geography and Ocean Sciences, Yanbian University, Yanji 133002, China

**Correpsondence to:* Mingyu Li*, email: leemy@ybu.edu.cn*

Abstract: Carbon emissions are a critical global issue requiring detailed spatial analyses to support regional carbon peak and neutrality strategies. This study investigates the spatiotemporal evolution and spatial differentiation of county-level land-use carbon emissions (CELU) in the Changchun-Jilin-Tumen (CJT) region from 2012 to 2021 by integrating land use data, nighttime light imagery, and socio-economic statistics with the Optimal Parameter Geodetector (OPGD) model. The analysis identifies key drivers of spatial emission variability, including construction land proportion (q-value: 0.8882), land area per capita (q-value: 0.7609), and urbanization rate (q-value: 0.5875), underscoring the significant role of land-use patterns and urbanization. Results show a 21.2% increase in CELU, from 67,594.46×10^4 t in 2012 to 81,942.35×10^4 t in 2021, with emissions concentrated in industrially active and urbanized western and southern counties, while forest-rich central and eastern counties exhibit lower emissions. Using the Grey Model (GM (1,1)), the study forecasts that CELU will rise from 78,484.364×10^4 t in 2022 to 88,985.198×10^4 t by 2030, reflecting a 14% increase over the forecast period. This trajectory highlights the misalignment between current trends and the region's goals of creating a "low-carbon industrial zone" and "livable cities," emphasizing the need for transitioning to renewable energy, optimizing industrial structures, and implementing sustainable land-use practices such as brownfield redevelopment and ecological land protection. By combining advanced remote sensing with nonlinear spatial analysis, this study offers a replicable high-resolution framework for understanding carbon emission drivers and spatial patterns, providing actionable insights for refining carbon reduction strategies and achieving sustainable development goals at both national and global scales.

Keywords: Land-use carbon emissions; Nighttime light data；Spatial emission drivers；OPGD model；Changchun-Jilin-Tumen region

1. Introduction

Global climate change has underscored the urgent need for effective carbon reduction strategies, as increasing atmospheric carbon dioxide levels contribute to severe environmental and economic consequences, including sea-level rise, extreme weather events, and disruptions to ecosystems and human livelihoods(Cui et al., 2020; Yan et al., 2022). Land-use changes, which are second only to fossil fuel combustion in their contribution to carbon emissions, significantly impact the global carbon cycle and regional ecosystems(Clark et al., 2018). As the world’s largest carbon emitter, China has committed to peaking its carbon emissions by 2030 and achieving carbon neutrality by 2060, highlighting the importance of regional and localized solutions that align economic development with sustainability goals(Yang & Li, 2023).

The Changchun-Jilin-Tumen (CJT) region in northeastern China presents a critical case for studying land-use carbon emissions due to its unique blend of socioeconomic and ecological characteristics. Beyond its strategic economic role as part of China's “Northeast Revitalization” initiative, the CJT region exemplifies diverse land-use patterns and development dynamics,

ranging from heavily industrialized plains in the west to forest-rich mountainous areas in the east. This regional diversity provides a valuable opportunity to analyze spatial variability in carbon emissions and evaluate the effectiveness of mitigation strategies across different land-use and urbanization contexts. Furthermore, the region's integration into national policies and its position as a hub for industrial and economic activities make it representative of broader trends in rapidly urbanizing and industrializing areas across the globe.

While significant research has explored carbon emissions at national, provincial, and municipal scales, localized analyses that capture fine-scale spatial variability and county-level dynamics remain limited. Studies such as Liu et al. (2019) have employed meta-frontier approaches to examine provincial-level drivers of carbon emissions but fail to address localized spatial heterogeneity. At the municipal level, Chen et al. (2021) leveraged nighttime light (NTL) data to estimate city-level emissions, demonstrating the utility of remote sensing but relying on econometric models that inadequately capture nonlinear spatial interactions. Similarly, Long et al. (2022) analyzed county-level variations in Wu'an City, providing valuable insights but utilizing traditional spatial econometric approaches that often assume fixed spatial relationships and linearity.

Recent advancements in remote sensing technologies, particularly the use of NTL data, offer new possibilities for high-resolution spatial analyses. NTL data serve as reliable proxies for human activities such as energy consumption and urbanization, providing finer spatial and temporal resolutions than traditional statistical approaches(J. Chen et al., 2021). However, the integration of NTL data with advanced spatial models remains limited, reducing the capacity of existing studies to uncover the drivers of spatial emission variability.

This study addresses these gaps by integrating high-resolution NTL data with the Optimal Parameter Geodetector (OPGD) model to analyze spatial drivers of land-use carbon emissions in the CJT region from 2012 to 2021. The OPGD model's ability to uncover nonlinear relationships and spatial heterogeneity is further complemented by the Grey Model (GM (1,1)), which forecasts carbon emission trends for 2022–2030. This research not only bridges the gap in county-level emission studies but also provides actionable insights for regional carbon management strategies. Moreover, by situating the findings within the context of global emission reduction efforts, the study offers a replicable framework for other regions facing similar sustainability challenges, contributing to both national and international climate goals.

2. Materials and methods

2.1. Study Area

The Changchun-Jilin-Tumen Development and Opening-up Pilot Zone (hereafter the "Changchun-Jilin-Tumen Region") is located in Northeast China, strategically positioned at the center of Northeast Asia along the New Eurasian Land Bridge. This 73,000 km² region spans from 124°30′47″E–131°19′29″E and 42°00′02″N–44°56′46″N (*Fig. 1*) and includes parts of Changchun City (central urban areas, Dehui, and Nongan), Jilin City (Jiaohe and Yongji), and the entirety of Yanbian Korean Autonomous Prefecture, comprising 23 counties.

The region features a monsoon-influenced temperate climate, with hot, humid summers and cold, dry winters, and a varied topography ranging from mountainous terrain in the east to flat alluvial plains in the west and southeast(Wang et al., 2024). This diversity supports forests and arable land in the west, providing significant natural carbon sinks. However, rapid industrialization and urbanization have elevated energy consumption and carbon emissions, particularly in western counties.

By 2021, the region's GDP was 945.427 billion yuan, with contributions from primary (8.4%), secondary (40.4%), and tertiary (51.2%) sectors, reflecting its status as an economic hub. Its urbanization rate reached 60.23%, underlining the pressures of rapid development (Jilin Statistical Yearbook, 2022). The region's designation in 2009 as a national strategic priority under the "Planning Outline for the Development and Cooperation of the Tumen River Area" has accelerated industrial growth but also presents significant challenges in achieving carbon neutrality.

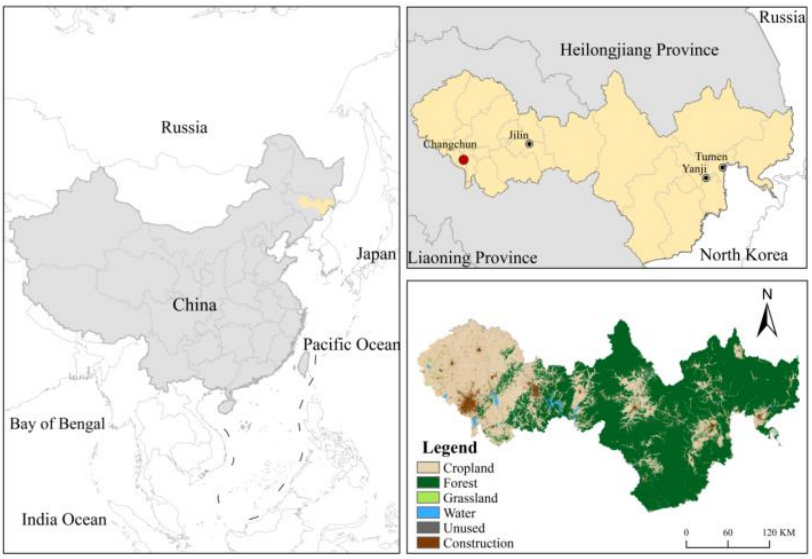

Fig. 1. Geographic Location of the Study Area.

2.2. Data Sources

This study integrated diverse datasets to analyze county-level land-use carbon emissions (CELU) in the Changchun-Jilin-Tumen region. The primary data sources are:

1. Land Use Data: The China Land Cover Dataset (CLCD) was processed on Google Earth Engine (GEE) using Landsat imagery and a random forest classifier. It categorizes land into six types: cultivated land, built-up land, forest, water bodies, grassland, and unused land, with a spatial resolution of 30 meters(Yang & Huang, 2021).

2. Nighttime Light Data: NPP-VIIRS-like NTL data (2012–2021), sourced from the National Earth System Science Data Center, provides high-resolution proxies for human activity and energy consumption(Z. Chen et al., 2021).

3. Energy and Socio-Economic Data: Data on energy consumption, GDP, population, and industrial outputs were obtained from provincial and municipal yearbooks.

4. Administrative Boundaries: Vector boundary data for 2023 was acquired from the Resources and Environmental Science Data Center.

A summary of the data types and their respective sources is provided in *Table 1*.

Table 1

Data Categories and Sources Used in the Study.

Data Type	Data Year	Data Source
NPP-VIIRS-like NTL data	2012-2021	National Earth System Science Data Center (http://www.geodata.cn)
CLCD Data	2012-2021	Wuhan University CLCD-LULC Product (https://zenodo.org/records)
Energy consumption data	2012-2021	http://www.stast.gov.cn

Population GDP Fixed Assets Primary industry output Secondary industry output	2012-2021	http://tjj.jl.gov.cn; http://www.jlcity.gov.cn; http://www.changchun.gov.cn/sycx; http://www.yanbian.gov.cn.
Administrative Boundaries	2023	Resources and Environmental Science Data Center (https://www.reesdc.cn)

2.3. Preprocessing of NPP-VIIRS-like NTL Data

The NTL dataset, formatted using the GCS_WGS_1984 coordinate system, spans 2012–2021 with a 500-meter resolution. Thresholding techniques removed outliers, ensuring temporal consistency and spatial accuracy. Masked extraction isolated data specific to the study area, aligning the analysis with China's administrative boundaries.

This preprocessing represents a methodological innovation, using NTL data as a robust proxy for energy consumption and human activity. By addressing spatial data gaps, it enables fine-scale carbon emission analysis in regions where detailed statistics are lacking.

2.4. Method

A comprehensive framework (*Fig. 2*) was developed to estimate county-level carbon emissions from land use (CELU) for the period 2012 to 2021. This framework integrates advanced data processing and spatial analysis techniques, ensuring rigorous assessment of both direct and indirect emissions.

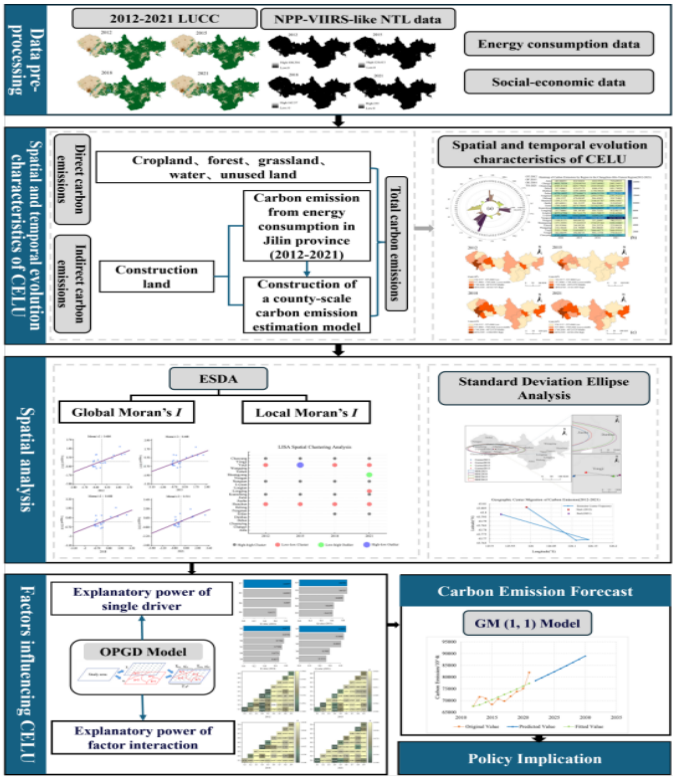

Fig. 2. Research Framework for Carbon Emission Analysis.

2.4.1. Carbon Emission Estimation

Carbon emissions were categorized into direct and indirect emissions, calculated using standardized approaches to ensure methodological consistency and comparability.

Direct Emissions

Direct emissions were derived from five land-use types: cultivated land, forest, grassland, water bodies, and unused land. The emissions were estimated using the equation:

$$E_1 = \sum_{i=1}^{n} C_i = \sum_{i=1}^{5} (S_i \times \partial_i) \quad (1)$$

Where E_c is the total direct carbon emissions, C_i represents the emissions from each land-use type, S_i is the area of each land type, ∂_i is the carbon emission (or absorption) coefficient (+ for carbon sources, − for carbon sinks), and *n* denotes the five land-use types (cultivated land, forest, grassland, water bodies, unused land).

The carbon emission coefficients (δi) applied in the calculations are shown in *Table 2*.

Table 2

Carbon Emission Coefficients for Land Use Types.

Land Use Type	Carbon Emission Coefficient (δi)	Unit	Reference
Cropland	0.422	t/hm^2	Li et al., 2018
Forest	-0.585	t/hm^2	Lai, 2010
Grassland	-0.021	t/hm^2	Yang et al., 2022
Water	-0.253	t/hm^2	Shi et al., 2019
Unused Land	-0.005	t/hm^2	Lai,2010

Indirect Emissions

Indirect emissions, primarily originating from built-up land, were calculated based on energy consumption data from 2012 to 2021, following methodologies from Niu et al. (2021) and Cai et al. (2023). These emissions include contributions from both energy consumption and electricity use, computed using the following equations:

1.Emissions from Energy Consumption (E_1):

$$E_1 = \sum_{i=1}^{8} (e_i \times A_i) \quad (2)$$

Where E_1 is the carbon emissions from energy consumption, e_i represents the quantity of energy consumed, and A_i is the emission coefficient for each energy type.

2.Emissions from Electricity Consumption (E_2):

$$E_2 = \sum_{i=1}^{n} (e_i \times B_i \times 10) \quad (3)$$

Where E_2 is the emissions from electricity consumption, e_i denotes the energy consumed (kWh), and B_i is the emission coefficient for electricity.

The carbon emission coefficients (A_i) used for energy types are presented in *Table 3*.

Table 3

CO_2 Emission Coefficients for Energy Types(Wang et al., 2020).

Energy Type	Carbon Emission Coefficient	Unit
Crude oil	3.0202	Kg CO_2/kg
Fuel oil	3.1705	Kg CO_2/kg
Kerosene	3.0719	Kg CO_2/kg
Natural oil	2.1622	Kg CO_2/m^3
Coal	1.9003	Kg CO_2/kg
Gasoline	2.9251	Kg CO_2/kg
Diesel	3.0959	Kg CO_2/kg
Coke	2.8604	Kg CO_2/kg
Electric power	1.0960	Kg $Kw^{-1}h^{-1}$

Spatial Allocation of Indirect Emissions

Indirect emissions were spatially distributed using nighttime light intensity data. This approach leveraged the strong linear correlation (r=0.9647, p<0.01) between total digital number (TDN) and carbon emissions in Jilin Province (*Table 4*). The formula used for spatial allocation is:

$$E_j = \frac{DN}{TDN} \times (E_1 + E_2) \quad (4)$$

Where E_j represents the estimated carbon emissions, DN is the nighttime light intensity, and TDN is the total digital number of the nighttime light data.

Table 4

Indirect Carbon Emissions and TDN Values in Jilin Province (2012–2021).

Year	Indirect Carbon Emissions(10^4t)	TDN Value
2012	98194.6608	184989.6125
2013	100008.3044	203832.7775
2014	100167.2943	186502.4340
2015	96673.1046	199240.8195
2016	97843.5369	216193.2913
2017	101713.8163	262317.5770
2018	105589.8589	283692.9399
2019	109592.3773	311268.8500
2020	111692.5068	330948.0100

2021	115877.2953	387662.9850

Total carbon emissions (E_{total}) were calculated as:

$$E_{total} = E_c + E_j \quad (5)$$

Where E_{total} represents the sum of direct and spatially localized indirect emissions.

2.4.2. Spatial Analysis

Exploratory Spatial Data Analysis (ESDA) identified spatial autocorrelation using Moran's I and LISA statistics. Standard Deviation Ellipse (SDE) analysis tracked the mean center and spatial distribution trends.

2.4.3 Geographical Factor Detection

The Optimal Parameters Geographical Detector (OPGD) model was applied to quantify the explanatory power of factors such as land use and urbanization. Parameter optimization was conducted using R's GD package, uncovering nonlinear interactions among variables.

2.4.4 Grey Prediction Model

To assess whether a dataset is suitable for grey prediction modeling, a level ratio test is performed on the original sequence to verify that the level ratios fall within a specified range. The original data sequence is represented as $X^{(0)} = [x^{(0)}(1), x^{(0)}(2), \ldots, x^{(0)}(n)]$, and the level ratios $\lambda(k)$ are calculated using the following formula:

$$\lambda(k) = \frac{x^{(0)}(k+1)}{x^{(0)}(k)} \quad (6)$$

If all calculated level ratios $\lambda(k)$ lie within the interval ($e^{-2/(n+1)}$, $e^{-2/(n+2)}$), where *n* is the sample size, the sequence is deemed suitable for grey prediction.

Based on the original sequence$X^{(0)}$, an accumulated sequence is generated by applying a cumulative sum, defined as:

$$X^{(1)}(k) = \sum_{i=1}^{k} x^{(0)}(i) \quad (7)$$

This produces a new sequence $X^{(1)} = [x^{(1)}(1), x^{(1)}(2), \ldots, x^{(1)}(n)]$, where *n* is the number of data samples. The mean sequence is then calculated as:

$$z^{(1)}(k) = \frac{1}{2}\left[x^{(1)}(k) + x^{(1)}(k-1)\right], \quad k = 2,3,\ldots,n. \quad (8)$$

The grey differential equation is constructed as:

$$x^{(0)}(k) + az^{(1)}(k) = b \quad (9)$$

From this, the development coefficient *a* and the grey effect coefficient *b* are determined.

The corresponding GM (1,1) whitened differential equation is given by:

$$\frac{dx^{(1)}}{dt} + az^{(1)}(t) = b \quad (10)$$

The discrete solution of the GM (1,1) model is expressed as:

$$\widehat{X^{(1)}}(k) = \left[x^{(0)}(1) - \frac{b}{a}\right] e^{-\alpha(k-1)} + \frac{b}{a} \quad (11)$$

The original sequence model is derived as:

$$\widehat{X^{(0)}}(k) = [x^{(0)}(1) - \frac{b}{a}]\, e^{-a(k-1)}(1 - e^{a}) \quad (12)$$

The model's accuracy is verified using the relative residual $\varepsilon(k)$, calculated as:

$$\varepsilon(k) = \left|\frac{x^{(0)}(k) - \widehat{x^{(0)}}(k)}{x^{(0)}(k)}\right| \quad (13)$$

If $\varepsilon(k)$<0.1, the prediction accuracy is classified as high. If $\varepsilon(k)$<0.2, the prediction accuracy is moderate.

A posterior error ratio test is performed using the posterior error ratio *C*, calculated as:

$$C = \frac{S_2}{S_1} \quad (14)$$

where:

$$S_1 = \sqrt{\frac{1}{n}\sum_{k-1}^{n}[x^{(0)}(k) - \bar{x}]^2} \quad , \quad S_2 = \sqrt{\frac{1}{n}\sum_{k=1}^{n}[\varepsilon(k) - \bar{\varepsilon}]^2} \quad (15)$$

If C<0.35, the model's predictive performance is deemed excellent; if 0.35≤C<0.5, the performance is considered good. These criteria provide a robust framework for assessing the suitability and reliability of the GM (1,1) model for predictive analysis.

3. Result

3.1. Temporal and Spatial Evolution of Land Use Carbon Emissions

3.1.1 Temporal Trends in Land Use Carbon Emissions

Between 2012 and 2021, the Changchun-Jilin-Tumen (CJT) region exhibited a consistent increase in land use carbon emissions and carbon emission density (*Fig. 3*). Total net carbon emissions rose from 67,594.46×10⁴ t in 2012 to 81,942.35×10⁴ t in 2021, reflecting a growth rate of over 21%. This trend is closely associated with urbanization and industrialization, which increased energy demand across sectors such as construction, transportation, and manufacturing. Simultaneously, the carbon sequestration capacity of forests and grasslands proved insufficient to counterbalance emissions stemming from the expansion of built-up land. In rural areas, improved living standards, supported by initiatives such as targeted poverty alleviation and rural revitalization, further contributed to higher emissions.

At the county level, Nanguan District experienced the largest increase in carbon emissions, from 10,314.71 × 10⁴ t in 2012 to 16,518.18 × 10⁴ t in 2021. Conversely, Wangqing County recorded the smallest increase, with emissions rising only marginally from 154.18 × 10⁴ t to 210.71 × 10⁴ t over the same period. Notably, some areas reported decreases in emissions. For instance, carbon emissions in Chuanying District declined from 4,003.71 × 10⁴ t in 2012 to 2,464.79 × 10⁴ t in 2021. Similarly, emissions in Fucheng District decreased from 3,355.71 × 10⁴ t to 2,391.91 × 10⁴ t, while Longtan District experienced a reduction from 4,072.67 × 10⁴ t to 2,108.43 × 10⁴ t. These declines were primarily driven by industrial restructuring, which replaced traditional high-carbon industries with lower-carbon sectors such as services and technology. Adoption of cleaner energy technologies, increased reliance on renewable energy, and the closure of outdated industrial facilities further supported emission reductions.

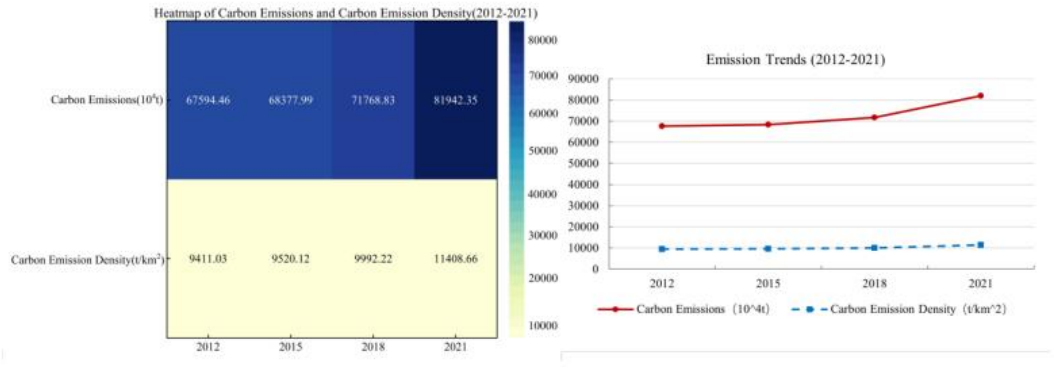

Fig. 3. Carbon Emissions and Carbon Emission Density in the Changchun-Jilin-Tumen Region (2012–2021).

3.1.2 Spatial Variation of Land Use Carbon Emissions

This study employed the Natural Breaks method to classify land use carbon emissions in the Changchun-Jilin-Tumen (CJT) region into four categories: low-carbon zones, lower-middle carbon zones, middle carbon zones, and high-carbon zones. Spatial visualization using ArcGIS and Origin revealed distinct spatial patterns and temporal trends in carbon emissions（*Fig. 4*）.

Carbon emissions consistently displayed a pattern of higher emissions in the southwest, particularly in urbanized and industrialized areas, and lower emissions in the central and eastern regions, characterized by lower population density and greater vegetation coverage. In 2012, the region comprised 8 low-carbon zones, 5 lower-middle carbon zones, 5 middle carbon zones, and 5 high-carbon zones. High-emission areas, such as Kuancheng, Lvyuan, Nanguan, Erdao, and Chaoyang districts, were linked to intensive industrial activities, high population density, and advanced infrastructure, which contributed to elevated energy consumption and emissions. In contrast, districts like Helong City, Wangqing County, and Tumen City experienced significantly lower emissions due to a focus on low-carbon industries such as cultural tourism, food production, and healthcare, alongside high forest and grassland coverage that supported carbon sequestration.

From 2015 to 2018, carbon emissions rose across most districts. The number of low-carbon zones decreased, while middle-carbon zones increased to 8, reflecting a shift in spatial patterns. Middle-carbon zones such as Jilin City, Yanji City, Hunchun City, and Shuangyang District emerged as key contributors, driven by industrial and power generation activities. These areas, often located near high-carbon zones, demonstrated the influence of urbanization and economic activity on regional emissions. High-carbon zones, however, remained stable during this period.

By 2021, the distribution of emission zones became more uniform, with 5 zones in each category. While overall emissions continued to rise, temporary reductions in some districts were observed, likely due to the economic slowdown and restricted industrial activities caused by the global health crisis. These disruptions highlighted the sensitivity of emission trends to external factors, such as global economic conditions.

The spatial patterns and trends in carbon emissions underscore the influence of land use and human activity on regional carbon dynamics. High-emission areas were consistently associated with urbanization and industrialization, while lower-emission areas benefitted from natural carbon sequestration provided by forest and grassland cover. These findings reveal critical spatial disparities in carbon emissions, which provide a foundation for understanding the environmental impacts of land use and economic activities in the CJT region.

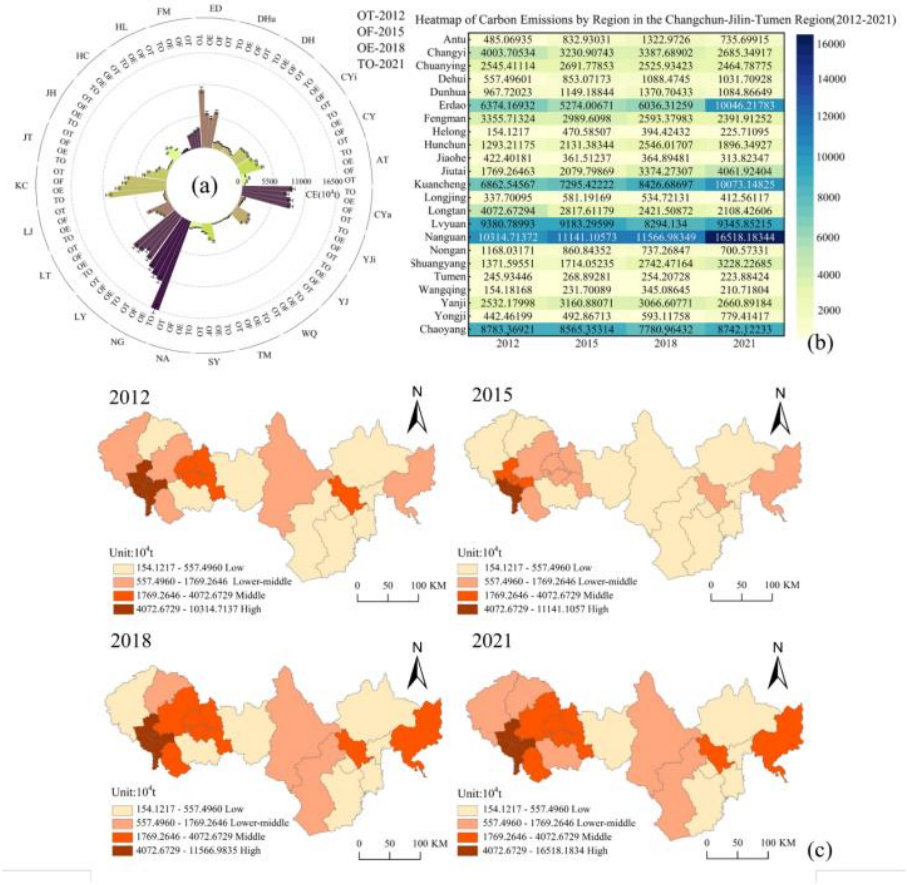

Fig. 4. Spatial and Temporal Characteristics of Carbon Emissions from Land Use.

(a) Net carbon emissions across years.

(b) Heatmap analysis of carbon emissions (2012–2021).

(c) Evolution of spatial patterns of carbon emissions (2012–2021).

Note: Abbreviations for regions: 'AT' - Antu; 'CY' - Changyi; 'CYi' - Chuanying; 'DH' - Dehui; 'Dhu' - Dunhua; 'ED' - Erdao; 'FM' - Fengman; 'HL' - Helong; 'HC' - Hunchun; 'JH' - Jiaohe; 'JT' - Jiutai; 'KC' - Kuancheng; 'LJ' - Longjing; 'LT' - Longtan; 'LY' - Lvyuan; 'NG' - Nanguan; 'NA' - Nongan; 'SY' - Shuangyang; 'TM' - Tumen; 'WQ' - Wangqing; 'YJ' - Yanji; 'YJi' - Yongji; 'CYa' - Chaoyang.

3.2. Spatial Agglomeration Characteristics

3.2.1 Global Moran's I Index

Using the adjacency spatial weight matrix, the Global Moran's I values for county-level land use carbon emissions were calculated with GeoDa software. The results, presented in *Fig. 5*, indicate that the Moran's I values for 2012, 2015, 2018, and 2021 were 0.486, 0.468, 0.488, and 0.511, respectively. All values were positive and statistically significant at the 99% confidence level.

These results demonstrate a trend characterized by an initial decrease in Moran's I, followed by an increase, reflecting changes in the spatial clustering of counties with similar carbon emission levels in the Changchun-Jilin-Tumen region. Despite fluctuations, the overall pattern indicates that the region remains spatially clustered throughout the study period.

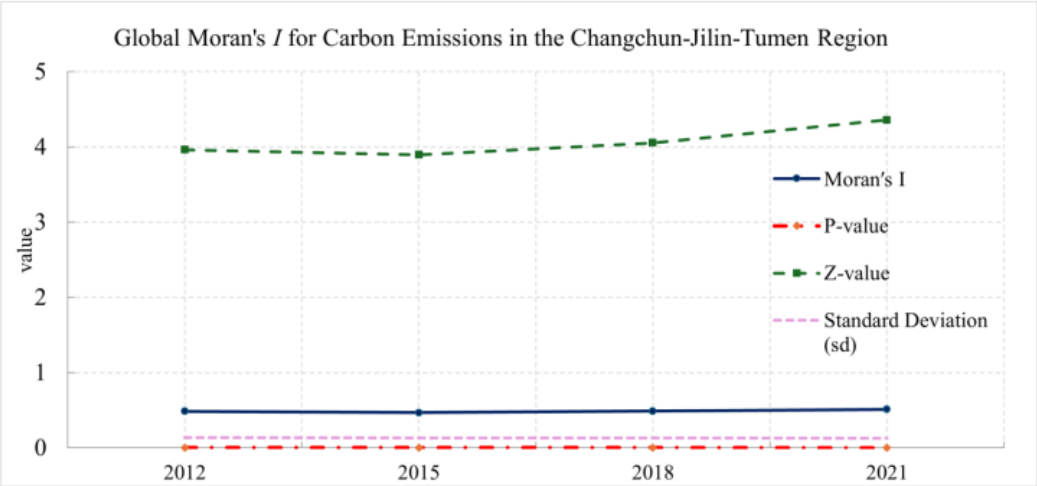

Fig.5 Global Moran's *I* for Carbon Emissions in the Changchun-Jilin-Tumen Region（2012-2021）.

3.2.2 Local Spatial Autocorrelation Patterns (LISA Analysis)

From 2012 to 2021, the spatial clustering patterns in the Changchun-Jilin-Tumen region remained relatively stable, as illustrated in *Fig. 6*. High-high (H-H) and low-low (L-L) clustering were the dominant patterns, reflecting the spatial distribution of carbon emissions across districts. Specific high-low (H-L) and low-high (L-H) clustering areas were also identified during the study period.

High-High (H-H) Clustering:

H-H clusters were primarily located in districts with moderate to high carbon emissions, such as Nanguan, Chaoyang, Erdao, and Kuancheng. These districts, situated in the core urban areas of Changchun, are characterized by advanced urbanization, significant population density, and integrated industrial structures. Dominant land-use types in these regions, including built-up and cultivated land, contributed substantially to carbon emissions, forming concentrated high-emission clusters.

Low-Low (L-L) Clustering:

L-L clusters were mainly observed in districts with low to moderately low carbon emissions, including Hunchun, Yanji, and Longjing. These areas are predominantly covered by forests and grasslands, characterized by low population densities and economies reliant on tourism, light industry, and services. The presence of substantial natural carbon sinks and minimal industrial activities significantly reduced carbon emissions in these districts.

High-Low (H-L) Clustering:

H-L clustering was observed in Yanji in 2015, where high-emission districts were surrounded by low-emission regions. This pattern reflects a reliance on coal-fired boilers during the transition to cleaner energy sources such as electricity and natural gas. The incomplete shift to clean energy during this period sustained coal boilers as a significant source of carbon emissions.

Low-High (L-H) Clustering:

L-H clustering occurred in Shuangyang in 2021, where low-emission areas were surrounded by high-emission districts. Shuangyang's primary land use is agricultural, which generates relatively low emissions compared to urbanized and industrialized regions. However, its proximity to high-emission zones resulted in a localized low-emission cluster within a broader high-emission region.

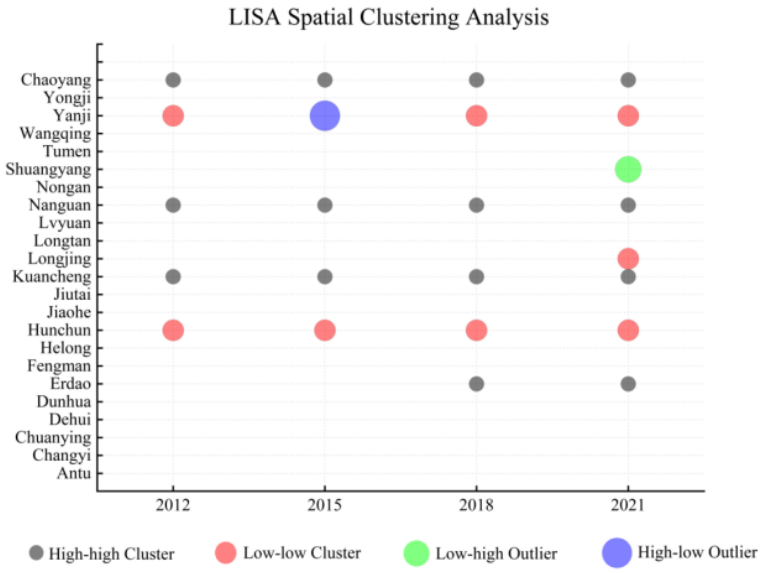

Fig. 6. LISA Clustering Map of Land Use Carbon Emissions in the Study Area (2012-2021).

3.3. Centroid Migration Characteristics

The standard deviation ellipse method was utilized to analyze the spatial distribution and evolutionary trends of land-use carbon emissions. This method provides insights into the spatial extension, integration, and other regional distribution characteristics. *Table 5* and *Fig. 7* highlight key patterns in carbon emissions.

The standard deviation ellipse of net land-use carbon emissions in the Changchun-Jilin-Tumen region exhibits an east-west orientation, with the centroid located between 125°55'41"E–126°08'24"E and 43°46'05"N–43°48'22"N, southwest of the region's geometric center. This positioning reflects higher carbon emissions in the southwestern areas (*Fig. 7*).

3.3.1 Principal Axis and Dispersion Trends

From 2012 to 2015, the major axis length increased from 141.272 km to 163.159 km, and the minor axis length grew from 34.916 km to 36.8 km. Between 2015 and 2018, the major axis expanded further to 165.928 km, and the minor axis to 38.446 km, indicating a continued east-west dispersion. This pattern aligns with regional integration policies aimed at fostering development across the area. From 2018 to 2021, the major axis contracted to 141.302 km, and the minor axis decreased to 35.264 km, signaling a concentration of emissions along the east-west axis.

The azimuth angle fluctuated slightly, increasing from 90.692° in 2012 to 91.710° in 2015, peaking at 91.893° in 2018, and then declining to 91.126° in 2021. These values, consistently within 90°–92°, indicate the overall stability of the spatial orientation of carbon emissions during the study period.

The area of the ellipse expanded from 15,491 km² in 2012 to a peak of 20,034 km² in 2018, followed by a contraction to 15,649 km² in 2021. This reflects a peak in spatial dispersion in 2018, followed by a period of concentration.

3.3.2 Centroid Migration Analysis

The trajectory of centroid migration demonstrates an initial southeastward shift (2012–2015), followed by a northwestward shift (2018–2021), with a total migration distance of 30.214 km over the 10-year period. Between 2012 and 2015, the centroid moved 0.12° eastward and 0.038° southward, covering 10.521 km. From 2015 to 2018, it shifted 0.029° eastward and 0.0008° southward, spanning 2.409 km. The largest migration occurred between 2018 and 2021, with the centroid moving 0.211° westward and 0.029° northward over 17.284 km.

Despite these shifts, the carbon emission centroid remained within Yongji County, concentrating in the western and southwestern parts of the CJT region. These areas, dominated by built-up and cultivated land, are significant emission hotspots due to energy-intensive secondary industries, rapid urbanization, and economic growth. Policies favoring resource allocation to these areas have further contributed to their high emission levels.

3.3.3 Implications for Carbon Emission Control

The findings highlight the need to prioritize emission reduction efforts in the western and southern urban areas of the CJT region. Industrial restructuring and enhanced energy efficiency are essential to mitigate emissions in these carbon-intensive zones and support sustainable development.

Table 5

Characteristics of Carbon Emission Standard Deviation Ellipse in the Changchun-Jilin-Tumen Region.

Year	Longitude (°E)	Latitude (°N)	Distance (km)	Major axis(km)	Minor axis(km)	Rotation (°)	Area (km^2)
2012	125°59'23"	43°48'22"	-	141.2720	34.9160	90.6920	15491
2015	126°06'36"	43°46'05"	10.5210	163.1590	36.8000	91.7100	18855
2018	126°08'24"	43°46'08"	2.4090	165.9280	38.4460	91.8930	20034
2021	125°55'41"	43°47'53"	17.2840	141.3020	35.2640	91.1260	15649

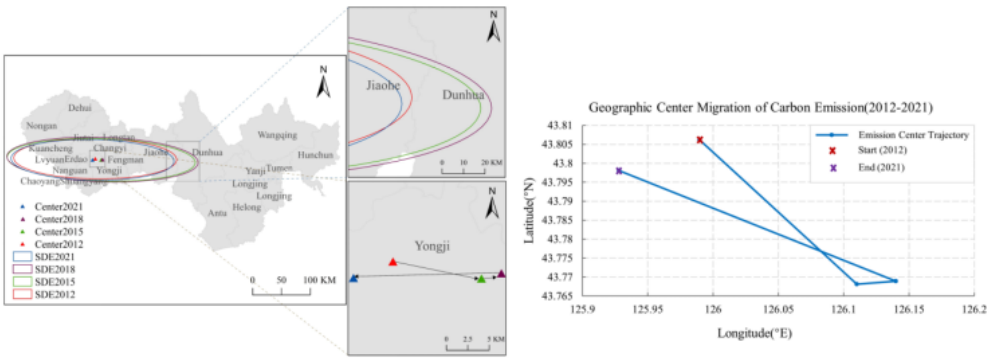

Fig. 7. Standard Deviation Ellipse Parameters and Trajectory of Centroid Migration for Carbon Emissions in the Changchun-Jilin-Tumen Region (2012–2021).

3.4. Analysis of Factors Influencing Land Use Carbon Emissions

The spatial variability of land-use carbon emissions (CELU) at the county level in the Changchun-Jilin-Tumen region is significant. To investigate the mechanisms driving this variability, a geographic detector model was applied to analyze influencing factors and their interactions. Nine explanatory variables were selected based on prior research and data availability, as detailed in *Table 6*.

Table 6

Indicators of Factors Influencing Land Use Carbon Emissions.

Element Layer	Indicator Layer
Energy intensity	X1：Energy consumption per GDP (t/10,000yuan)
Economic development	X2：Per capita GDP (yuan)
Industrial structure	X3：Proportion of primary industry output X4：Proportion of secondary industry output
Regional investment	X5：Fixed asset Investment (million yuan)
Land use scale	X6：Land area per capita(persons/km^2)
Land-use structure	X7：Construction land proportion
Population size	X8：Population size (person)
Urban development	X9：Urbanization rate

3.4.1. Detection of influential factors

The analysis identified significant variations in the explanatory power (q-values) of factors influencing CELU spatial differentiation. To address these variations, multiple discretization methods—such as natural breaks, equal intervals, and quantile classification—were applied using the "GD" package in R. Optimal parameter combinations were selected based on the highest q-values (*Fig. 8*).

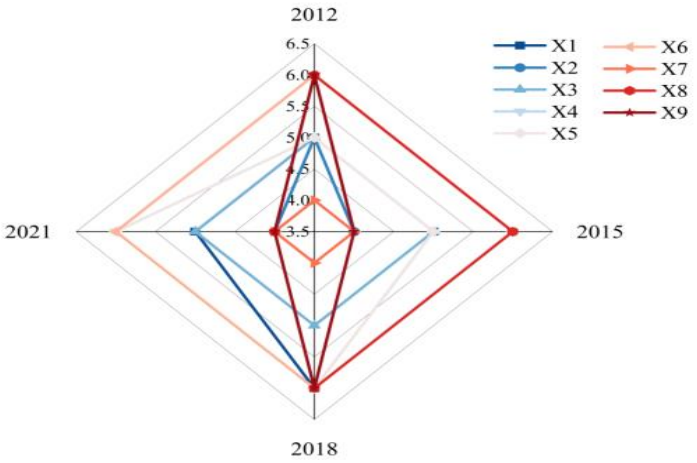

Fig. 8. Parameter Optimization for Explanatory Variables of Land Use Carbon Emissions Using the OPGD Model.

The optimized results revealed that the most influential factors (q > 0.5) were X7 (Construction land proportion), X3 (Proportion of primary industry output), X6 (Land area per capita), X9 (Urbanization rate), and X8 (Population size) (*Table 7*). Among these, X7 consistently exhibited the highest explanatory power across all years, underscoring its dominant role in driving emissions. The significant contribution of construction activities reflects their energy-intensive nature. Factors such as X3, X6, X9, and X8 also demonstrated substantial explanatory power, emphasizing the role of land-use patterns, urbanization, and population size in shaping emissions.

Secondary factors, including X2 (Per capita GDP), X1 (Energy consumption per GDP), and X5 (Fixed asset investment),

exhibited moderate explanatory power. X4 (Proportion of secondary industry output) consistently showed the lowest q-values, suggesting a limited impact on CELU, potentially due to fluctuations in industrial activity or the effectiveness of policy interventions.

Table 7

Explanatory Power of Factors Influencing Land Use Carbon Emissions.

Detection Indicator	Explanatory Power				
	2012	2015	2018	2021	Average
X1	0.3815	0.3966	0.7206***	0.2588	0.4394
X2	0.4619*	0.2401	0.4620	0.8082***	0.4931
X3	0.8953***	0.8727***	0.8772***	0.8606***	0.8765
X4	0.3859	0.3449	0.1653	0.2394	0.2839
X5	0.3773	0.4748*	0.3360	0.4589	0.4118
X6	0.8870***	0.8099***	0.7564***	0.5902**	0.7609
X7	0.8977***	0.8735***	0.8758***	0.9056***	0.8882
X8	0.6171**	0.6295**	0.6774**	0.2677	0.5479
X9	0.5482*	0.6125***	0.6677**	0.5215**	0.5875

Note: Statistical significance is denoted as ***p < 0.01, **p < 0.05, *p < 0.1.

3.4.2. Interaction Factor Detection Results

Interaction detection was conducted to evaluate the synergistic effects of overlapping factors, as shown in *Fig. 9*. Most interactions exhibited two-factor enhancement or nonlinear enhancement, with q-values for combined factors consistently exceeding those of individual factors. This indicates that CELU spatial differentiation is shaped by the interplay of multiple factors.

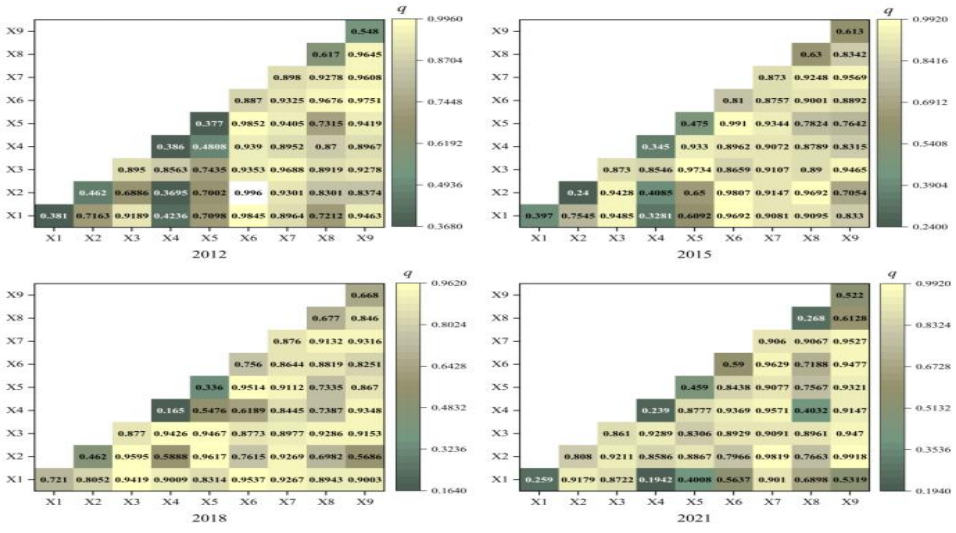

Fig. 9. Interaction Detection Results for Factors Influencing CO_2 Emissions in the Changchun-Jilin-Tumen Region.

For example, the interaction between X6 (Land area per capita) and X2 (Per capita GDP) produced the highest q-value of 0.9960 in 2012, reflecting a strong synergistic effect. Similarly, in 2015, the interaction between X6 and X5 (Fixed asset investment) achieved a q-value of 0.9910, highlighting the combined influence of land use and regional investment. In 2018, the interaction between X2 and X5 yielded a q-value of 0.9918, underscoring the interconnectedness of economic growth and investment. By 2021, the interaction between X2 and X9 (Urbanization rate) achieved a q-value of 0.9918, illustrating the combined impact of urbanization and economic development.

Even factors with lower individual q-values, such as X1 (Energy consumption per GDP), demonstrated strong interactive effects when paired with other variables. For instance, the interaction between X1 and X2 yielded a q-value of 0.798, indicating the amplified role of energy efficiency when combined with economic growth. In contrast, nonlinear weakening effects were observed in some cases, such as between X1 and X7, suggesting that improvements in energy efficiency can mitigate emissions associated with urban expansion.

These findings demonstrate that CELU in the CJT region is influenced by a complex interplay of factors, with interactions frequently amplifying their combined effects. Integrated policies accounting for the synergistic relationships between urbanization, land use, economic growth, and industrial activity are essential for addressing spatial variability in emissions and achieving regional carbon reduction targets.

3.5 Carbon Emission Forecast and Analysis

In May 2022, the National Development and Reform Commission of China introduced the *National Climate Change Adaptation Strategy 2035*, which emphasizes comprehensive control of greenhouse gas emissions and the development of an enhanced policy framework for climate adaptation. Aligning with these national objectives of carbon peaking and neutrality, the People's Government of Jilin Province launched the *14th Five-Year Comprehensive Energy Conservation and Emission Reduction Implementation Plan*. Within this context, the Changchun-Jilin-Tumen region, as a pilot area, carries a critical responsibility in driving carbon reduction efforts.

This study investigates carbon emissions from land use in the Changchun-Jilin-Tumen region from 2012 to 2021, employing the grey model (GM (1,1)) to forecast emissions for the period 2022–2030. The results provide insights into regional carbon emission trends and inform strategies for achieving dual carbon goals.

3.5.1 Model Construction and Validation

The carbon emission time series data, with level ratios ranging from 0.1281 to 1.0573, were deemed suitable for GM (1,1) model construction. The development coefficient (a=−0.0157) and the grey effect coefficient (b=66,550.24) were derived during the modeling process. Validation demonstrated a posterior error ratio (C=0.0266) well below the threshold of 0.36, indicating excellent prediction accuracy. Furthermore, the model exhibited a maximum relative error of 0.0465, reaffirming its robustness and reliability for forecasting carbon emissions. These metrics confirm the GM (1,1) model as an appropriate tool for analyzing and predicting carbon emission trends in the region.

3.5.2 Forecast Results

The forecast indicates a steady increase in carbon emissions within the Changchun-Jilin-Tumen region from 2022 to 2030. Emissions are projected to rise from $78{,}484.364\times10^4$ t in 2022 to $88{,}985.198\times10^4$ t by 2030, reflecting a net increase of 10.5×10^6 t over this period. Compared to 2012, when emissions were $67{,}594.462\times10^4$ t, this represents a 31.6% increase in emissions by 2030 (*Fig. 10*).

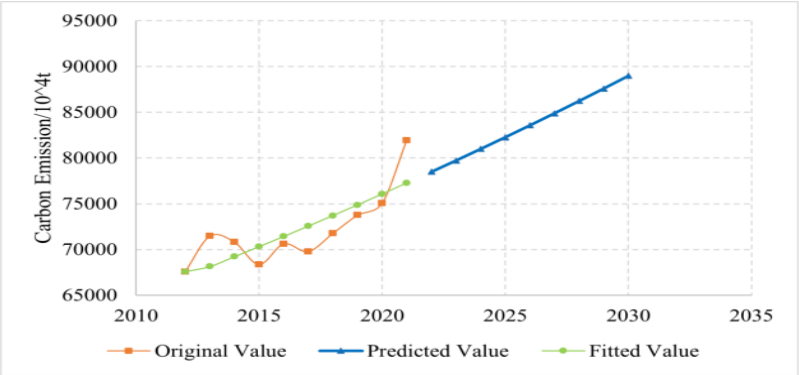

Fig.10. Prediction of Land Use Carbon Emissions in Changchun-Jilin-Tumen from 2022 to 2030.

The results highlight a significant misalignment with the region's stated goals of developing a "low-carbon industrial zone" and "livable cities." The upward trajectory underscores the necessity for more effective measures to curb emissions and accelerate progress toward carbon neutrality.

Efforts to achieve dual carbon targets must focus on implementing comprehensive environmental regulations, particularly targeting high-energy consumption sectors. Optimizing the industrial structure is critical, requiring a transition from traditional energy-intensive industries to low-carbon and green industries to address emissions at their source. At the same time, expanding the adoption of renewable energy sources—such as solar, wind, and biomass—is essential to meet growing energy demands sustainably while reducing carbon output.

Additionally, investments in pollution control technologies and environmental infrastructure are vital for enhancing carbon management capabilities. For instance, adopting carbon capture and storage (CCS) technologies in industrial facilities and modernizing energy grids could significantly mitigate emissions. Regulatory enforcement should be complemented by financial incentives for industries adopting low-carbon practices, ensuring alignment with regional and national sustainability goals.

4. Discussion

4.1. Temporal and Spatial Trends of Land Use Carbon Emissions

This study provides a detailed county-level analysis of land use carbon emissions (CELU) in the Changchun-Jilin-Tumen region, addressing gaps in existing research, which predominantly focuses on national or provincial scales. While large-scale analyses are essential for identifying general patterns, the localized approach adopted here enhances the precision of policy recommendations and enables more targeted carbon reduction strategies.

The results show a consistent increase in CELU, from 67,594.46 × 10^4 t in 2012 to 81,942.35 × 10^4 t in 2021. This rise is largely attributed to urbanization, industrial growth, and construction land expansion. Policies such as the Northeast Revitalization Strategy and the Tumen River Area Development Plan have supported economic development but have also exacerbated carbon emissions. A temporary decline in emissions during the COVID-19 pandemic highlights the sensitivity of carbon outputs to economic disruptions, suggesting that structural economic adjustments could have significant impacts on emission trajectories.

Spatially, high-emission areas are concentrated in western and southern counties, driven by energy-intensive industries and urbanization, whereas lower emissions are observed in forest-rich eastern regions. These findings align with global trends observed in industrialized regions such as the Yangtze River Delta and the Guangdong-Hong Kong-Macao Greater Bay Area, where urban agglomerations are characterized by high energy demands and concentrated emissions(Chen et al., 2023; Zhang et al., 2023; Zhou et al., 2018).

In comparison, regions such as the Beijing-Tianjin-Hebei area show similar spatial clustering due to industrial hubs and high population densities(Yan et al., 2022). However, the Changchun-Jilin-Tumen region is distinguished by its reliance on primary industries and emerging urban centers, necessitating tailored strategies that combine industrial restructuring with sustainable urbanization.

Persistent spatial clustering, as identified through Moran's I analysis, underscores the necessity of region-specific mitigation strategies tailored to local drivers and hotspots of emissions. These strategies could serve as a model for other developing regions facing similar challenges, particularly those in Southeast Asia or Latin America, where urban growth and industrial activities are accelerating.

4.2. Influencing Factors of Land Use Carbon Emissions

The Optimal Parameters Geographical Detector (OPGD) model provides detailed insights into the primary factors influencing CELU. As shown in *Table 7,* the proportion of construction land (X7) consistently exhibits the highest explanatory power, with Q values ranging from 0.8735 in 2015 to 0.9059 in 2021. This underscores the significant impact of urban expansion on emissions, particularly in western counties where built-up land growth has increased energy demands for heating, lighting, and industrial production (*Fig. 11*).

Primary industry output (X3) is another critical driver, with notable Q values in 2012 (0.8953) and 2018 (0.8772). This indicates that agricultural activities, including fertilizer and pesticide use, as well as land reclamation, contribute significantly to CELU. Addressing these emissions requires promoting sustainable agricultural practices and improving land management.

In comparison to regions like the Yangtze River Delta, where secondary and tertiary industries dominate carbon emissions, the Changchun-Jilin-Tumen region's reliance on primary industries calls for unique mitigation strategies. For instance, optimizing agricultural practices and reducing emissions from rural energy consumption could significantly contribute to emission reduction goals.

Interaction analysis reveals that synergistic effects between factors, such as urbanization and per capita GDP, amplify their combined impact on emissions. This highlights the need for integrated strategies that address these interactions. For example, promoting mixed-use development and vertical urban expansion can limit land-use sprawl while meeting urban growth demands. Such approaches could be adapted to international contexts, such as rapidly urbanizing regions in Africa and South Asia, to manage emissions while supporting economic development.

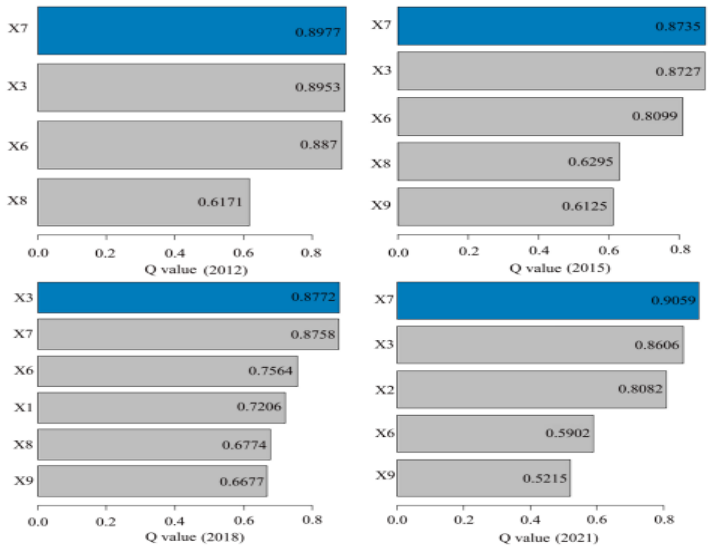

Fig. 11. Factor Detection Results for Land Use Carbon Emissions Using the OPGD Model

4.3. Carbon Emission Forecast and Analysis

To address global climate change and support China's carbon peak and neutrality goals, Jilin Province has implemented the *Carbon Emission Reduction Implementation Plan*. As a key pilot region for development and openness, the Changchun-Jilin-Tumen (CJT) region holds significant responsibility in these efforts. This study analyzes carbon emissions from land use in the CJT region from 2012 to 2022 and employs the Grey Model (GM (1,1)) to forecast emissions from 2022 to 2030. The results provide critical insights into the carbon reduction challenges faced by the region.

The findings indicate that carbon emissions in the CJT region are expected to continue rising during the forecast period. Emissions are projected to increase from 78,484.364×10^4 t in 2022 to 88,985.198×10^4 t by 2030, representing a growth rate of 14%. This upward trend reflects ongoing pressures from economic expansion and highlights the need for enhanced carbon mitigation measures.

To align with national carbon peak and neutrality objectives, stricter and more effective emission reduction policies are essential, particularly in high-emission sectors. Strengthening support for green and low-carbon industries, optimizing industrial structures, and expanding the adoption of renewable energy are critical steps. Promoting low-carbon technologies and improving energy efficiency within enterprises are also necessary measures. While economic growth may lead to a short-term increase in urban land-use carbon emissions, achieving sustainable development will require coordinated efforts across government, enterprises, and society.

Further research is needed to refine and validate the forecast model to better simulate long-term changes in carbon emissions. Such refinements will provide more robust tools for policymakers to plan and implement effective carbon reduction strategies.

4.4. Policy implications

Achieving carbon neutrality in the Changchun-Jilin-Tumen region requires a systematic and multi-layered approach that integrates localized governance, innovative policy tools, and lessons from international best practices. County-level carbon monitoring systems should be established to enhance the precision of emission data and facilitate evidence-based policy adjustments. These systems can leverage advanced technologies, such as satellite-based remote sensing, IoT sensors, and AI-driven analytics, to track emissions in real time. For example, deploying smart meters to monitor industrial emissions can provide granular insights into emission hotspots, enabling precise intervention strategies. International experiences, such as Germany's municipal-level carbon monitoring frameworks under the European Green Deal, highlight the benefits of integrating monitoring platforms with regional governance to ensure effective and timely responses to emissions management challenges (European Commission, 2020).

Land-use planning is another critical area for addressing emissions. Effective land-use policies should focus on limiting the expansion of construction land in high-emission counties while promoting vertical urban development and brownfield redevelopment. Such measures not only reduce the pressure on greenfield sites but also accommodate urban growth in a sustainable manner. Introducing carbon taxes on land conversion from agricultural or forested areas to urban use could disincentivize sprawl, while offering subsidies for high-density, mixed-use developments can encourage vertical urban growth. Singapore provides an exemplary model, where strict zoning laws and incentives for vertical development have minimized land use without compromising economic or population growth（Urban Redevelopment Authority (URA)，2022）.

Transforming the industrial sector is vital for mitigating emissions in western high-emission regions. Incentivizing industries to adopt clean technologies and renewable energy through targeted policies, such as green subsidies and low-interest loans, can significantly reduce industrial carbon intensity. Additionally, implementing carbon pricing mechanisms and cleaner production standards aligns with successful strategies observed in the Yangtze River Delta and the Guangdong-Hong Kong-Macao Greater Bay Area(Sun & Miao, 2022; Wu, 2023). These regions have demonstrated that financial and regulatory incentives can encourage industrial sectors to adopt low-carbon innovations and renewable energy sources. Furthermore,

Denmark's national policies integrating renewable energy into industrial operations offer valuable insights, showing how coordinated government action can drive sector-wide transformation（Danish Energy Agency, 2020）.

In the eastern counties, which are dominated by forested landscapes, conservation and restoration efforts are crucial to enhancing their function as natural carbon sinks. Policies such as Payment for Ecosystem Services (PES) can provide financial incentives to local communities for maintaining and restoring forested areas. Forest carbon offset programs could also be introduced, enabling industries to fund afforestation and reforestation projects in exchange for carbon credits. Brazil's Amazon conservation initiatives serve as a useful reference, illustrating how international funding mechanisms and stringent deforestation controls can enhance forest preservation efforts（Brazilian Ministry of the Environment，2022）. These strategies align with China's broader ecological conservation goals while contributing to global carbon sink enhancement.

Lastly, fostering integrated collaboration among urban planners, industrial stakeholders, and policymakers is essential for developing comprehensive strategies that address the multifaceted drivers of emissions. Establishing cross-sectoral governance frameworks, such as regional carbon councils, can facilitate the alignment of local, regional, and national policies. The European Green Deal provides an effective model for such integration, where partnerships between local governments and private enterprises have successfully advanced green infrastructure projects（European Commission，2020). Drawing from these international practices, the Changchun-Jilin-Tumen region can design collaborative frameworks that align economic development with environmental sustainability, contributing to China's dual-carbon goals while setting a benchmark for other developing regions globally.

4.5. Contributions and Limitations

This study advances existing methodologies by combining nighttime light data with the OPGD model, offering significant improvements in spatial resolution and accuracy. Nighttime light data, a reliable proxy for human activity and energy consumption, enables high-resolution spatial analyses, while the OPGD model identifies key emission drivers and their interactions. This approach overcomes traditional methods' limitations by capturing fine-scale spatial heterogeneity and detecting nonlinear relationships among influencing factors. It also offers a replicable framework for other regions with similar data constraints, contributing to global carbon neutrality efforts.

However, some limitations remain. Nighttime light data, while effective for energy-related emissions, may underestimate emissions from agricultural and forestry activities. Additionally, the temporal scope of this study (2012–2021) may not fully reflect the long-term impacts of recent policy interventions or structural changes in energy consumption. Future research could extend the analysis period, incorporate cross-regional comparisons, and test the proposed methodologies in other international contexts, such as emerging economies or densely populated urban agglomerations.

5. Conclusion

This study investigates the spatiotemporal evolution and spatial differentiation of county-level land use carbon emissions (CELU) in the Changchun-Jilin-Tumen region from 2012 to 2021, integrating land use data, nighttime light imagery, and socio-economic statistics with the Optimal Parameter Geodetector (OPGD) model. The findings reveal a 21.2% increase in CELU, from 67,594.46×10^4 t in 2012 to 81,942.35×10^4 t in 2021. Emissions are concentrated in western and southern counties with significant industrial activity and urbanization, whereas forest-rich central and eastern counties exhibit lower emissions. The primary drivers of CELU are the proportion of construction land (q-value: 0.8882), land area per capita (q-value: 0.7609), and urbanization rate (q-value: 0.5875), underscoring the critical role of land-use patterns and urbanization in shaping spatial emission variability.

Building on these results, the Grey Model (GM (1,1)) predicts that CELU will continue to rise, from 78,484.364×10^4 t in 2022 to 88,985.198×10^4 t by 2030, reflecting a 14% increase over the forecast period and a 31.6% rise compared to 2012 levels. This upward trend highlights the misalignment between current trajectories and the region's goals of establishing a "low-carbon

industrial zone" and "livable cities." Addressing these challenges requires targeted measures, including transitioning to renewable energy and high-tech industries, optimizing industrial structures, and limiting the expansion of construction land in high-emission areas. Land-use optimization through brownfield redevelopment and ecological land protection, combined with stricter zoning regulations, will further support sustainable urban development.

To accelerate emission reductions, the government must prioritize technological innovation through subsidies, tax incentives, and public-private partnerships, fostering the adoption of energy-efficient technologies. Pilot programs for smart grids and sustainable urban designs can enhance mitigation efforts, while public awareness campaigns and incentives for low-carbon lifestyles are essential for encouraging community-level participation. This study provides a replicable high-resolution analytical framework for understanding carbon emission drivers and spatial patterns. Its adaptability enables application to other regions and future timeframes, offering insights for refining emission reduction strategies. By implementing evidence-based measures, the Changchun-Jilin-Tumen region can serve as a model for achieving balanced economic growth and sustainability, contributing to both national and global climate goals.

Declaration of Conflicting Interests

The author(s) declared no potential conflicts of interest with respect to the research, author-ship, and/or publication of this article.

Data Sharing Agreement

The data used in this study is publicly available, obtained through self-retrieval from public websites, and has been organized and processed. Therefore, specific data links cannot be provided.

Funding

The author(s) received no financial support for the research, authorship, and/or publication of this article.

References

1. Brazilian Ministry of the Environment. (2022). Action Plan for the Prevention and Control of Deforestation in the Legal Amazon (PPCDAm). https://www.gov.br/mma/en
2. Cai, W., & Ye, P. (2022). Does carbon emission trading improve low-carbon technical efficiency? Evidence from China. *Sustainable Production and Consumption*, *29*, 46-56. https://doi.org/10.1016/j.spc.2021.09.024
3. Chen, C., Luo, Y., Zou, H., & Huang, J. J. E. (2023). Understanding the driving factors and finding the pathway to mitigating carbon emissions in China's Yangtze River Delta region. *278*, 127897. https://doi.org/10.1016/j.energy.2023.127897
4. Chen, J., Gao, M., Cheng, S., Liu, X., Hou, W., Song, M.,…Fan, W. (2021). China's city-level carbon emissions during 1992–2017 based on the inter-calibration of nighttime light data. *Scientific Reports*, *11*(1), 3323. https://doi.org/10.1038/s41598-021-81754-y
5. Chen, Z., Yu, B., Yang, C., Zhou, Y., Yao, S., Qian, X.,…Wu, J. (2021). An extended time series (2000–2018) of global NPP-VIIRS-like nighttime light data from a cross-sensor calibration. *Earth Syst. Sci. Data*, *13*(3), 889-906. https://doi.org/10.5194/essd-13-889-2021
6. Clark, R., Reed, J., & Sunderland, T. J. L. u. p. (2018). Bridging funding gaps for climate and sustainable development: Pitfalls, progress and potential of private finance. *71*, 335-346. https://doi.org/10.1016/j.landusepol.2017.12.013
7. Cui, Y., Schubert, B. A., & Jahren, A. H. (2020). A 23 m.y. record of low atmospheric CO2. *Geology*, *48*(9), 888-892. https://doi.org/10.1130/G47681.1
8. Danish Energy Agency. (2020). Danish Climate Policies: Overview and Objectives.https://ens.dk/en/our-responsibilities/energy-climate-politics/danish-climate-policies
9. European Commission. (2020). A European Green Deal: Striving to be the First Climate-Neutral Continent. https://ec.europa.eu/info/strategy/priorities-2019-2024/european-green-deal

10. Jilin Statistics Bureau. (2022). Jilin Statistical Yearbook. http://tjj.jl.gov.cn/tjsj/tjnj/2022/ml/indexc.htm
11. Lai, L. (2010). Carbon Emission Effect of Land Use in China. *Nanjing University*.
12. Li, Y., Li, S., & Qi, J. (2018). Influencing factors on carbon emissions of land uses and analysis of their decoupling effects in Shaanxi province. *Research of Soil Water Conservation*, *25*(1), 382-390. https://doi.org/10.13869/j.cnki.rswc.2018.01.057
13. Liu, B., Shi, J., Wang, H., Su, X., & Zhou, P. (2019). Driving factors of carbon emissions in China: A joint decomposition approach based on meta-frontier. *Applied Energy*, *256*, 113986. https://doi.org/10.1016/j.apenergy.2019.113986
14. Long, Z., Pang, J., Li, S., Zhao, J., Yang, T., Chen, X.,…Wang, B. (2022). Spatiotemporal variations and structural characteristics of carbon emissions at the county scale: a case study of Wu'an City. *Environmental Science and Pollution Research*, *29*(43), 65466-65488. https://doi.org/10.1007/s11356-022-20433-5
15. Niu Y, Zhao X, Hu Y. (2021). Spatial variation of carbon emissions from county land use in Chang-Zhu-Tan area based on NPP-VIIRS night light. *Acta Scientiae Circumstantiae*, 41, 3847-3856. https://doi.org/10.13671/j.hjkxxb.2021.0281.
16. Shi, K., Yu, B., Zhou, Y., Chen, Y., Yang, C., Chen, Z., & Wu, J. (2019). Spatiotemporal variations of CO2 emissions and their impact factors in China: A comparative analysis between the provincial and prefectural levels. *Applied Energy*, *233-234*, 170-181. https://doi.org/10.1016/j.apenergy.2018.10.050
17. Sun, C., & Miao, B. (2022). Performance Evaluation of Reducing Consumption of Energy in the Yangtze River Delta under the Background of Low-Carbon Economy. *2022*(1), 3235776. https://doi.org/10.1155/2022/3235776
18. Urban Redevelopment Authority (URA). (2022). Planning in Singapore: Concept Plan and Master Plan. https://www.ura.gov.sg/Corporate/Planning
19. Wang, Y., Li, M., & Jin, G. (2024). Optimizing spatial patterns of ecosystem services in the Chang-Ji-Tu region (China) through Bayesian Belief Network and multi-scenario land use simulation. *Science of The Total Environment*, *917*, 170424. https://doi.org/10.1016/j.scitotenv.2024.170424
20. Wang, Y., M, T. D., T, Z. J., N, M., L, H. B., & Y, O. Z. (2020). The impact of urbanization on carbon emissions: Analysis of panel data from 158 cities in China. *Acta Ecologica Sinica*, *30*(21), 7897-7907. https://doi.org/10.586/stxb201911292591
21. Wu, Q. (2023). Theoretical Evaluation of Photovoltaic Thermal Water Source Heat Pump, Application Potential and Policy Implications: Evidence from Yangtze River Economic Belt, China. *15*(18), 13638. https://doi.org/10.3390/su151813638
22. Yan, H. M., Guo, X., Zhao, S. Q., & Yang, H. C. (2022). Variation of Net Carbon Emissions from Land Use Change in the Beijing-Tianjin-Hebei Region during 1990-2020. *LAND*, *11*(7), Article 997. https://doi.org/10.3390/land11070997
23. Yang, J., Zhang, M., Duo, L., Xiao, S., & Zhao, Y. (2022). Spatial Pattern of Land Use Carbon Emissions and Carbon Balance Zoning in Jiangxi Province. *Research of Environmental Sciences*, *35*(10), 2312-2321. https://doi.org/10.13198/j.issn.1001-6929.2022.05.04
24. Yang, J., & Huang, X. (2021). 30 m annual land cover and its dynamics in China from 1990 to 2019. *Earth System Science Data Discussions*, *13*(8), 3907-3925. https://doi.org/10.5194/essd-13-3907-2021
25. Yang, Y., & Li, H. (2023). Spatiotemporal dynamic decoupling states of eco-environmental quality and land-use carbon emissions: A case study of Qingdao City, China. *Ecological Informatics*, *75*, 101992. https://doi.org/10.1016/j.ecoinf.2023.101992
26. Zhang, X., Tang, Y., Han, H., & Chen, Z. J. S. (2023). Evolution Characteristics and Main Influencing Factors of Carbon Dioxide Emissions in Chinese Cities from 2005 to 2020. *15*(20), 14849. https://doi.org/10.3390/su152014849
27. Zhou, Y., Shan, Y., Liu, G., & Guan, D. J. A. e. (2018). Emissions and low-carbon development in Guangdong-Hong Kong-Macao Greater Bay Area cities and their surroundings. *228*, 1683-1692. https://doi.org/10.1016/j.apenergy.2018.07.038